Comparing Models for Diffusion in Supercooled Liquids: The Eutectic Composition of the Ag−Cu Alloy†

Charles F. Vardeman II and J. Daniel Gezelter*

Department of Chemistry and Biochemistry, University of Notre Dame, Notre Dame, Indiana 46556

Received: September 29, 2000; In Final Form: December 13, 2000

We present a comparison between the Continuous Time Random Walk (CTRW) model for dispersive transport and Zwanzig's model of self-diffusion in liquids using the cage correlation function as a means for obtaining the characteristic hopping times. This comparison was done using a realistic model for the interactions between metal atoms in a system that is known to form metallic glasses. We find that although the CTRW model uses a pathological model for the distribution of waiting times, the predictions of this theory are much closer to the actual diffusion constants than those obtained via Zwanzig's model. We also find that there is a simple linear relationship between the stretching parameter (β) for Kohlrausch−Williams−Watts decay of the cage correlation function and the dispersion parameter (γ) that characterizes the "fractal" distribution of waiting times in the CTRW model.

1. Introduction

Solid solutions of silver and copper near the eutectic point have been historical curiosities since Roman emperors used them to cut the silver content in the ubiquitous *denarius* coin by plating copper blanks with the eutectic mixture.[1] Curiosity in this alloy continues to the current day since the discovery that it forms a glassy material when rapidly quenched from the melt. The eutectic composition (60.1% Ag, 39.9% Cu) was the first glassy metal reported by Duwez in 1960.[2] The Duwez experiments give us an upper bound on the cooling rate required ($\approx 10^6$K/s) in this alloy, whereas other metallic glasses (based on Ti−Zr alloys) can be formed with cooling rates of only 1 K/s.[3] There is clearly a great wealth of information waiting to be discovered in the vitrification and crystallization of liquid alloys.

The Ag−Cu alloy is also of great theoretical interest because it resembles a model glass-forming Lennard−Jones system that has correlation functions that decay according to the famous Kohlrausch−Williams−Watts (KWW) law

$$C(t) \approx A \exp\left[-(t/\tau)^{\beta}\right] \tag{1}$$

Kob and Andersen observed stretched exponential decay of the van Hove correlation function in a system comprising an 80/20 mixture of particles with different well depths ($\epsilon_{AA} \neq \epsilon_{BB}$) and different range parameters ($\sigma_{AA} \neq \sigma_{BB}$).[4,5] They found that at low temperatures, the best fitting value for the stretching parameter β was approximately 0.8. The same system was later investigated by Sastry, Debenedetti, and Stillinger.[6] They observed nearly identical stretching parameters in the time dependence of the self-intermediate scattering function $F_s(k,t)$.[7]

In single component Lennard−Jones systems, the stretching parameters appear to be somewhat lower. Angelani et al. have reported $\beta \approx {}^1/_2$ for relatively low-temperature Lennard−Jones clusters, and Rabani et al. have reported similar values for the decay of correlation functions in defective Lennard−Jones crystals.

There have been a few recent studies of amorphous metals using fairly realistic potentials and molecular dynamics methodologies. Gaukel and Schober studied diffusion in $Zr_{67}Cu_{33}$,[8] and Qi et al. have looked at the static properties ($g(r)$, $s(\mathbf{k})$, etc.) for alloys of Cu with both Ag and Ni.[9] None of the metallic liquid simulation studies have observed time correlation functions in the supercooled liquid near T_g. It would, therefore, be interesting to know whether these realistic models have the same anomalous time dependence as the Lennard−Jones systems and, if so, whether their stretching behavior is similar to that observed in the two-component Lennard−Jones systems.

Additionally, bi-metallic alloys present an ideal opportunity for us to apply the cage-correlation function methodology that one of us developed to study the hopping rate in supercooled liquids.[10−13] In particular, we want to use it to test two models for diffusion, both of which use hopping times that are easily calculated by observing the long-time decay of the cage correlation function. The two models are Zwanzig's model,[14] which is based on the periodic interruption of harmonic motions around inherent structures, and the Continuous Time Random Walk (CTRW) model,[15−18] which can be used to derive transport properties from a random walk on a regular lattice where the time between jumps is nonuniform.

2. Theory

In this section, we give a brief introduction to the models for diffusion that we will be comparing, as well as a brief description of how one can use the cage-correlation function to obtain hopping rates in liquids.

2.1 Zwanzig's Model. In his 1983 paper[14] on self-diffusion in liquids, Zwanzig proposed a model for diffusion that consisted of "cells" or basins in which the liquid's configuration oscillates until it suddenly finds a saddle point on the potential energy surface and jumps to another basin. This model was based on and supported by simulations done by Stillinger and Weber,[19−22] in which the liquid configurations generated by molecular dynamics were quenched periodically by following the steepest descent path to the nearest local minima on the potential energy

† Part of the special issue "William H. Miller Festschrift".

10.1021/jp0035784 CCC: $20.00
Published on Web 01/31/2001

surface. Stillinger and Weber found that as their simulations progressed, the quenched configurations were stable for short periods of time and then suddenly jumped (with some recrossing) to other configurations.[20]

The starting point in Zwanzig's theory is the Green−Kubo formula[7,23] for the self-diffusion constant

$$D = \frac{1}{3}\int_0^\infty dt\langle \mathbf{v}(t)\cdot\mathbf{v}(0)\rangle \tag{2}$$

where $\langle \mathbf{v}(t)\cdot\mathbf{v}(0)\rangle$ is the time-dependent velocity autocorrelation function. Zwanzig's model predicts the diffusion constant using τ, the lifetime that characterizes the distribution ($\exp(-t/\tau)$) of residence times in the cells.

Following a jump, the coherence of the harmonic oscillations is disrupted, so all correlations between velocities will be destroyed after each jump. Zwanzig writes the velocity autocorrelation function in terms of the velocities of the normal modes in the nearest cell. The normal-mode frequencies are characterized by the normalized distribution function $\rho(\omega)$, and the time integral can be solved assuming the time dependence of a damped harmonic oscillator for each of the normal modes. In the continuum limit of normal-mode frequencies, one obtains

$$D = \frac{kT}{M}\int_0^\infty d\omega\rho(\omega)\frac{\tau}{(1+\omega^2\tau^2)} \tag{3}$$

where M is the mass of the particles.

Zwanzig does not explicitly derive the inherent structure normal modes from the potential energy surface (he used the Debye spectrum for $\rho(\omega)$). Moreover, the theory avoids the problem of how to estimate the lifetime τ for cell jumps that destroy the coherent oscillations in the sub-volume. Nevertheless, the model fits the experimental results quite well for the self-diffusion of tetramethylsilane (TMS) and benzene over large ranges in temperature.[24,25]

2.2 CTRW Model. In the CTRW model,[15−18] random walks take place on a regular lattice but with a distribution of waiting times

$$\psi(t) \approx \begin{cases} (t/\tau)^{-1-\gamma} & 0 < \gamma < 1 \\ \dfrac{1}{\tau}e^{-t/\tau} & \gamma = 1 \end{cases} \tag{4}$$

between jumps. $\gamma = 1$ represents normal transport, whereas $\gamma < 1$ represents transport in a "fractal time" regime. In this regime, the number of jumps grows in time t as t^γ and not linearly with time. This dependence implies that the jumps do not possess a well-defined mean waiting time and that there is no way to define a hopping rate for systems that are operating in the fractal time regime. (The two functional forms for the waiting time distribution appear odd at first, but they are connected smoothly by way of their Laplace transforms

$$\psi(u) = \left(\frac{1}{\tau} + u^\gamma\right)^{-1} \tag{5}$$

The inverse transform of this function results in the exponential form when $\gamma = 1$, and in the second form when $\gamma < 1$.)

Klafter and Zumofen have derived probability distributions for transport in these systems.[16] In the $\gamma = 1$ limit, they obtain the standard diffusive behavior in which the diffusion constant is inversely proportional to τ and proportional to the square of the lattice spacing for the random walk (σ_0)

$$D = \frac{\sigma_0^2}{6\tau} \tag{6}$$

This behavior is also suggested by our estimates of τ in CS_2 and in Lennard−Jones systems using the cage correlation function.[11,12]

When $\gamma < 1$, the situation is somewhat more complex. The mean-square displacement can be approximated at long times as

$$\langle r^2(t)\rangle = \frac{4\sigma_0^2}{3\sqrt{\pi}}\left(\frac{t}{\tau}\right)^\gamma\left(\frac{2-\gamma}{\gamma}\right)^\gamma\frac{1}{(2-\gamma)^2}\Gamma\left(\frac{7}{2}-\gamma\right) \tag{7}$$

Note that there is no well-defined diffusion constant for transport that behaves according to this expression.

The waiting time distribution in eq 4 can be used to derive a sticking probability

$$\Phi(t) \approx 1 - \int_0^t dt'\,\psi(t') \tag{8}$$

which is the probability of not having made a jump until time t. The long-time behavior of this function should be directly related to the long-time behavior of the cage correlation function, which is essentially a measurement of the fraction of atoms that are still within their initial surroundings. For the $\gamma < 1$ case, the distribution of waiting times in eq 4 results in sticking probability that decays as $t^{-\gamma}$. This is a very different behavior than the KWW law (eq 1) that has been observed in the defective Lennard−Jones crystals.[12]

Ngai and Liu have asserted that the KWW decay law (eq 1) cannot be explained through the use of the waiting time distribution in eq 4.[26] Instead, they propose a distribution

$$\psi(t) = c\alpha t^{\alpha-1}e^{-ct^\alpha} \tag{9}$$

which can explain the experimentally observed decay. The form of the waiting time distribution in eq 4 is more amenable to analytical approaches to calculating transport behavior. Blumen, et al. have investigated both proposed functional forms for $\varphi(t)$ for recombination phenomena[15] and found that eq 9 leads to time-independent rates at longer times. All of the moments of the distribution in eq 9 are finite, so it would produce a Gaussian random walk at long times. Blumen, et al. conclude that in order to observe anomalous transport, waiting time distributions with pathological long-time tails are required. Indeed, a connection between the algebraic waiting time distribution in eq 4 and the KWW decay law can be made when the diffusing species are migrating defects.[27−29]

2.3 Cage Correlation Function. In a recent series of papers,[10−13,30,31] one of us has been investigating approaches to calculating the hopping rate ($k_h = 1/\tau$) in liquids, supercooled liquids, and defective crystals. To obtain this estimate, we introduced the *cage correlation function*, which measures the rate of change of atomic surroundings and associates the long-time decay of this function with the basin hopping rate for diffusion. The details on calculating the cage correlation function can be found in Refs 10 and 11, but we will briefly review the concept here.

An atom's immediate surroundings are best described by the list of other atoms in the liquid that make up the first solvation shell. When a diffusive barrier crossing involving the atom has occurred, the atom has left its immediate surroundings. Following the barrier crossing, it will have a slightly different group of atoms surrounding it. If one were able to paint identifying

numbers on each of the atoms in a simulation and to keep track of the list of numbers that each atom could see at any time, then the barrier crossing event would be evident as a substantial change in this list of neighbors.

The cage correlation function uses a generalized neighbor list to keep track of each atom's neighbors. If the list of an atom's neighbors at time t is identical to the list of neighbors at time 0, the cage correlation function has a value of 1 for that atom. If any of the original neighbors are *missing* at time t, it is assumed that the atom participated in a hopping event, and the cage correlation function is 0. The atom's surroundings can also change due to vibrational motion, but at longer times, the cage will reconstitute itself to include the original members. Only those events which result in irreversible changes to the surroundings will cause the cage to decorrelate at long times. The mathematical formulation of the cage correlation function is given in Refs 10 and 11.

Averaging over all atoms in the simulation and studying the decay of the cage correlation function gives us a way to measure the hopping rates directly from relatively short simulations. We have used the cage correlation function to predict the hopping rates in atomic[10] and molecular[11] liquids, as well as in defective crystals.[12,13] In the defective crystals, we found that the cage correlation function, after being corrected for the initial vibrational behavior at short times, decayed according to the KWW law (eq 1) with a stretching parameter $\beta \approx {}^1/_2$. Angelani et al. have also reported $\beta \approx {}^1/_2$ for relatively low temperature Lennard−Jones clusters. This is notably different behavior from the correlation functions calculated for the Lennard−Jones mixtures that have been studied by Kob and Andersen,[4,5] and Sastry et al.[6] In this system, the stretching parameter was closer to 0.8.

This paper will concentrate on the use of the cage correlation function to obtain hopping times for use by the Zwanzig and CTRW models for diffusion in the Ag_6Cu_4 melt. We are also looking for the presence of anomalous dynamical behavior in the supercooled liquid at temperatures just above the glass transition to confirm the behavior observed in the simpler Lennard-Jones system. Section 3 will outline the computational methods used to perform the simulations. Section 4 contains our results, and section 5 concludes.

3. Computational Details

Several different pseudo-atom models have been developed that reasonably describe potentials in transition metals. In particular, the Embedded Atom Model (EAM)[32] and Sutton-Chen (SC)[33] potentials have been used to study a wide range of phenomena in metals.[34−36] Both potentials are based on a similar model of a liquid metal, which treats the nuclei and core electrons as pseudo-atoms embedded in the electron density due to the valence electrons on all of the other atoms in the system. The SC potential takes the simplest form

$$U_{\mathrm{tot}} = \sum_i \left[\frac{1}{2} \sum_{j \neq i} D_{ij} V_{ij}^{\mathrm{pair}}(r_{ij}) - c_i D_{ii} \sqrt{\rho_i} \right] \qquad (10)$$

where V_{ij}^{pair} and ρ_i are given by

$$V_{ij}^{\mathrm{pair}}(r) = \left(\frac{\alpha_{ij}}{r_{ij}} \right)^{n_{ij}}, \quad \rho_i = \sum_{j \neq i} \left(\frac{\alpha_{ij}}{r_{ij}} \right)^{m_{ij}} \qquad (11)$$

V_{ij}^{pair} is a repulsive pairwise potential that accounts for interactions of the pseudo-atom cores. The $\sqrt{\rho_i}$ term in eq 10 is an attractive many-body potential that models the interactions between the valence electrons and the cores of the pseudo-atoms. D_{ij}, D_{ii}, c_i, and α_{ij} are parameters used to tune the potential for different transition metals. The SC formulation of a metallic potential is advantageous because it closely resembles the form of the ubiquitous Lennard−Jones potential. This resemblance allows for the use of standard mixing rules in simulations of alloys.

We have chosen the Sutton−Chen potential with the same parametrization as Qi et al.[9] These parameters were obtained via empirical and ab initio calculations to match structural features of the fcc crystal.

To study the long-time portions of the correlation functions in this system without interference from the simulation methodology, we carried out molecular dynamics simulations in the constant-NVE ensemble. The density of the system was taken to be 8.742 g/cm^3. This density was chosen immediately to the liquid side of the melting transition from the constant thermodynamic tension simulations of Qi et al. Their simulations gave excellent estimates of phase and structural behavior, and should be seen as a starting point for investigations of these materials.

The equations of motion were integrated using the velocity Verlet integrator with a time step of 1 fs. A cutoff radius was used in which $r_{ij}^{\mathrm{cut}} = 2\alpha_{ij}$. Nine independent configurations of 500 atoms were generated by starting from an fcc lattice and randomly choosing the identities of the particles to match the Ag_6Cu_4 compsition, which is near the eutectic composition for this alloy.[37]

Each configuration was started at a temperature of 1350 K (well in excess of the melting temperature at this density) and then cooled in 50 K increments to 400 K. At each temperature increment, the systems re-sampled velocities from a Maxwell−Boltzmann distribution every ps for 20 ps, after which they were allowed to equilibrate for 50 ps. Following the equilibration period, we collected particle positions and velocities every ps for 250 ps. The lower temperature runs (375, 350, 325, and 300 K) were sampled for 500 ps, 1, 1, and 7 ns respectively to accumulate more accurate long-time statistics. Cooling in this manner leads to a effective quenching rate of approximately 10^{11} K/s. This quenching rate is much larger than those that are achieved through experimental methods, which typically are on the order of 10^6 or 10^7 K/s depending on the quenching method.[2]

4. Results

The simulation results were analyzed for several different structural and dynamical properties. Figure 1 shows the pair correlation function

$$g(r) = \frac{V}{N^2} \left\langle \sum_i \sum_{j \neq i} \delta(\mathbf{r} - \mathbf{r}_{ij}) \right\rangle \qquad (12)$$

at seven temperatures ranging from liquid to supercooled liquid. The appearance of a split second peak in the radial distribution function has been proposed as a signature of the glass transition.[38] This behavior is evident in Figure 1 for temperatures below 500 K.

Wendt and Abraham have proposed another structural feature to estimate the location of the glass transition. Their measure

$$R_{\mathrm{WA}} = \frac{g_{\mathrm{min}}}{g_{\mathrm{max}}} \qquad (13)$$

is the ratio of the magnitude of the first minimum, g_{min} to the

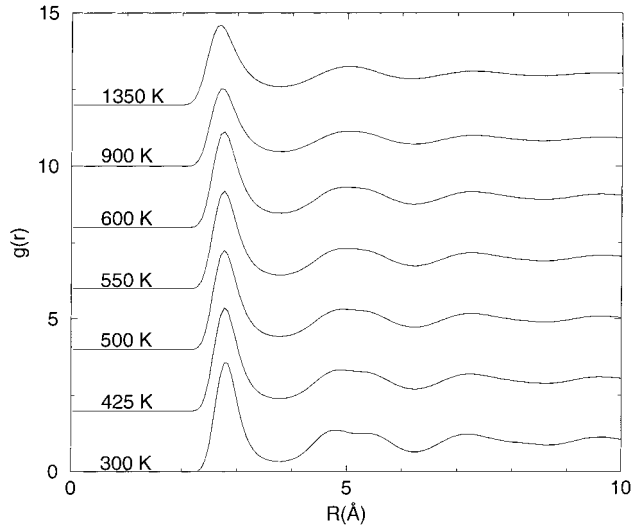

Figure 1. Radial distribution functions for Ag_6Cu_4. The appearance of the split second peak at 500 K indicates the onset of a structural change in the supercooled liquid at temperatures above T_g.

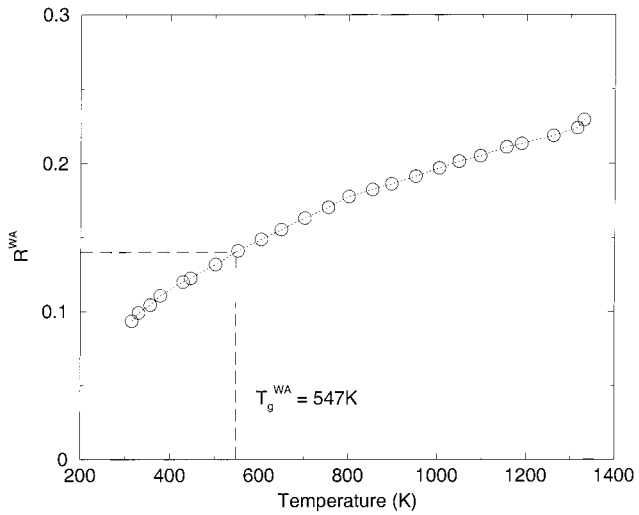

Figure 2. Wendt-Abraham parameter (R_{WA}) as a function of temperature. $T_g^{WA} \approx 540$ K for a cooling rate of 1.56×10^{11} K/s.

first maximum, g_{max} in the radial distribution function. According to their estimates, when the value of R_{WA} reaches 0.14, the system has passed through the glass transition.[39] We observed a T_g^{WA} of 547 K given a cooling rate of 1.56×10^{11} K/s. Goddard, et al. observed a $T_g^{WA} \approx 500$ K for a cooling rate of 2×10^{12} K/s in constant temperature, constant thermodynamic tension (*TtN*) simulations.[9]

We note that the split second peak in $g(r)$ appears at T_g^{WA}, a temperature for which the diffusion constant is still an appreciable fraction of it's value in the liquid phase. We also note that diffusive behavior continues at the lowest simulated temperature of 300 K indicating that glass transition for our system lies below 300 K. Taking the operational definition of the glass transition to be the temperature at which the viscosity exceeds 10^{13} poise,[38] it is obvious that neither of these structural factors should be considered a definitive marker of T_g. It has also been noted in previous papers that changes in these structural factors can occur in certain supercooled metallic liquids independently of glassy behavior.[40,41] However, both structural features seem to mark the onset of anomalous thermodynamic and dynamical behavior and should at best be taken as evidence of the location of the mode coupling theory (MCT) critical temperature, T_c, and not T_g itself.

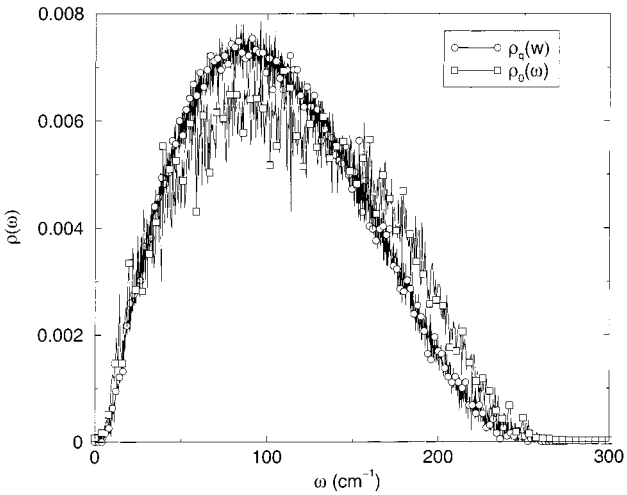

Figure 3. Density of states calculated from quenched normal modes, $\rho_q(\omega)$, and from the Fourier transform of the velocity autocorrelation function, $\rho_o(\omega)$.

To compute diffusion constants using Zwanzig's model (eq 3), one must obtain an estimate of the density of vibrational states ($\rho(\omega)$) of the liquid. We obtained the $\rho(\omega)$ in two different ways, first by quenching 20 high-temperature (1350 K) configurations to the nearest local minimum on the potential energy surface. These structures correspond to inherent structures on the liquid-state potential energy surface. Normal modes were then calculated for each of these inherent structures by diagonalizing the mass-weighted Hessian to give the squares of the normal-mode frequencies. The second method we used for determining the vibrational density of states was to compute the normalized power spectrum of the velocity autocorrelation function

$$\rho_0(\omega) = \int_{-\infty}^{\infty} \langle \mathbf{v}(t)\cdot\mathbf{v}(0)\rangle \, e^{-i\omega t}\, dt \qquad (14)$$

for trajectories which hover just above the inherent structures. To calculate the power spectrum, a small amount of kinetic energy (8 K) was given to each of the 20 inherent structures, and the system was allowed to equilibrate for 30 ps. After equilibration, the velocity autocorrelation functions were calculated from relatively short (30 ps) trajectories, and the density of states was obtained from a simple discrete Fourier transform. At this low temperature, the particles do not diffuse, so the velocity correlation function does not decay due to hopping. This implies that the Fourier transform of $\langle \mathbf{v}(t)\cdot\mathbf{v}(0)\rangle$ is 0 at $\omega = 0$

Both of these methods result in similar gross features for the density of states, but there are some important differences in their estimates at low frequencies. Notably, the normal mode density of states ($\rho_q(\omega)$) is missing some of the low-frequency modes at frequencies below 10cm^{-1}. The power spectrum ($\rho_0(\omega)$) recovers these modes but gives a much noisier estimate for the density of states.

We determined that with a radial cutoff of $2\alpha_{ij}$, the potential (and forces) exhibited a large number of discontinuities which made the minimization into the inherent structures somewhat challenging. In this type of potential, the discontinuities at the cutoff radius *cannot* be fixed by shifting the potential as is done with the Lennard−Jones potential. This limitation is due to the nonadditive nature of the density portion of the potential function. To address this problem, the minimizations and frequencies were obtained with a radial cutoff of $3\alpha_{ij}$, which provided a surface of adequate smoothness. The larger cutoff

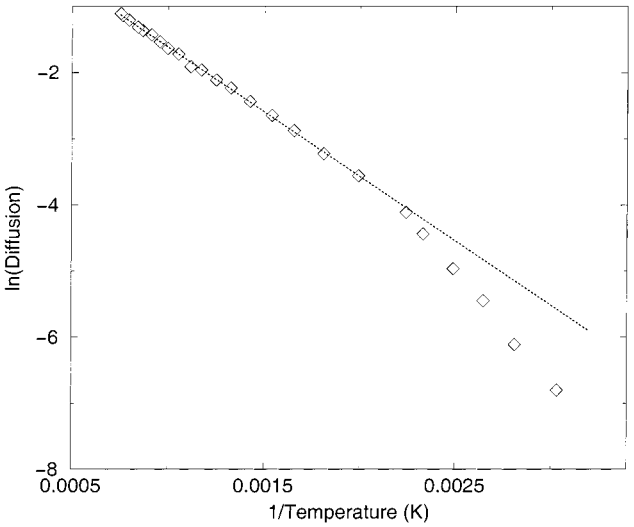

Figure 4. Arrhenius plot of the self-diffusion constants indicating significant deviation from Arrhenius behavior at temperatures below 450 K.

radius requires a larger system size, and so, for the minimizations and the calculation of the densities of states, we used a total of 1372 atoms.

We note that one possible way to provide a surface without discontinuities would be to use a shifted form of the density

$$\rho_i = \sum_{j \neq i} \left(\frac{\alpha_{ij}}{r_{ij}}\right)^{m_{ij}} - \left(\frac{\alpha_{ij}}{r_{ij}^{\text{cut}}}\right)^{m_{ij}} \tag{15}$$

This modification substantially alters the attractive portion of the potential and has a deleterious effect on the forces. A similar shifting in the Lennard−Jones or other pairwise-additive potential would not exhibit this problem. Although this modification does provide a much smoother potential, it would properly require a re-parametrization of c_i and D_{ii}, tasks which are outside the purview of the current work.

4.1 Diffusive Transport and Exponential Decay. Translational diffusion constants were calculated via the Einstein relation[23]

$$D = \lim_{t\to\infty} \frac{1}{6t} \langle |\mathbf{r}_i(t) - \mathbf{r}_i(0)|^2 \rangle \tag{16}$$

using the slope of the long-time portion of the mean square displacement. We show an Arrhenius plot of the natural logarithm of the diffusion constant vs $1/T$ in Figure 4.

The structural features that we noted previously (i.e., the split-second peak in $g(r)$ and T_g^{WA}) appear at the same temperature at which the log of the diffusion constant leaves the traditional straight-line Arrhenius plot.

Truhlar and Kohen have suggested an interpretation of this type of plot based on Tolman's interpretation of the activation energy.[42−44] Specifically, positive convexity in Arrhenius plots requires the average energy of all diffusing particles rise more slowly then the average energy of all particles in the ensemble with increasing temperature. This only occurs if the microcanonical-ensemble diffusion constant, $D(E)$, decreases with increasing energy. Truhlar and Kohen explain that one possible explanation of this behavior is if configuration space can be decomposed into two types of conformation, one which is "reactive" in which diffusive hopping occurs with a rate constant of $K_R(E)$, and one in which there is no diffusion. If the probability of being found in the reactive region is given by $P_R(E)$, then the overall diffusion constant

$$D(E) = P_R(E)\, K_R(E) \tag{17}$$

would allow $P_R(E)$ to decrease with E faster than $K_R(E)$ can increase. In other words, higher energy systems explore a larger segment of phase space and spend a smaller fraction of their time in regions where there is a probability of diffusive hopping. As the energy is decreased, more time is spent in regions of configuration space where diffusive hopping is allowed so $D(E)$ should increase with decreasing E.

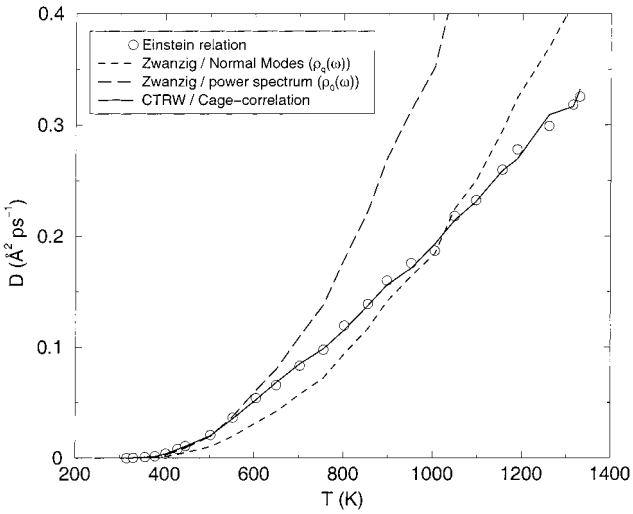

Figure 5. Self-diffusion constant for the two models under consideration compared to the values computed via standard techniques.

In Figure 5 , we show the diffusion constants calculated via the Einstein relation eq 16 along with results for the Zwanzig and CTRW ($\gamma = 1$) models using hopping times obtained from simple linear fits to the long-time decay of the cage correlation function. For Zwanzig's model, we show results using the two different estimates for the vibrational density of states. For the CTRW model, we have used a jump length (σ_0) of 1.016 Å for *all* temperatures shown.

Zwanzig's model is extremely sensitive to the low-ω portion of $\rho(\omega)$,[11] so it is no surprise that the choice of the density of states gives a large variation in the predicted results. The agreement with the diffusion constants is better at lower temperatures, but we observe an obviously incorrect temperature dependence in the higher temperature liquid regime.

The CTRW model with $\gamma = 1$ and an assumption of fixed jump distances gives much better agreement in the liquid regime, and the trend with changing temperature seems to be in excellent agreement with the Einstein relation.

Delving a bit more deeply into the CTRW predictions, we can assume that the distribution of hopping times is well behaved (i.e., $\gamma = 1$) but that the jump *distance* is temperature dependent. To obtain estimates of the jump distance as a function of temperature, $\sigma_0(T)$, we can invert (eq 6) by multiplying the cage-correlation hopping time by the self-diffusion constant. We show the temperature-dependent hopping distances in Figure 6. Note that these assumptions would lead us to believe that the average jump distance is increasing sharply as one approaches the glass transition, which could be an indicator of motion dominated by Levy flights.[17,18]

4.2 Nondiffusive transport and nonexponential decay

A much more realistic scenario is that the distribution of hopping *times* changes while the jump distance remains the same

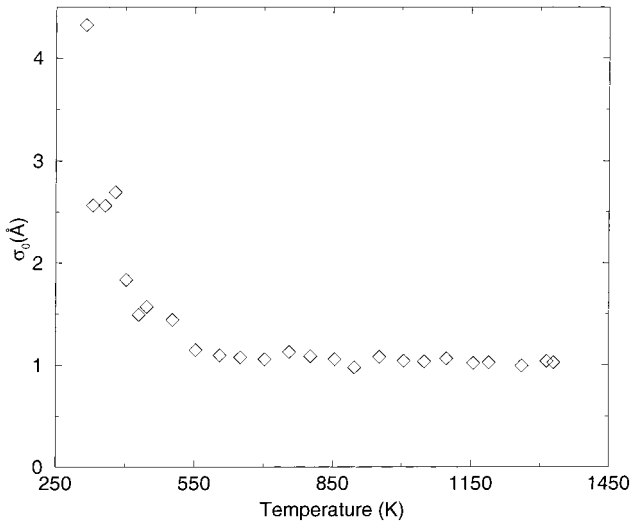

Figure 6. CTRW hopping distance, $\sigma_0(T)$, as a function of temperature assuming $\gamma = 1$ and using the cage correlation hopping times.

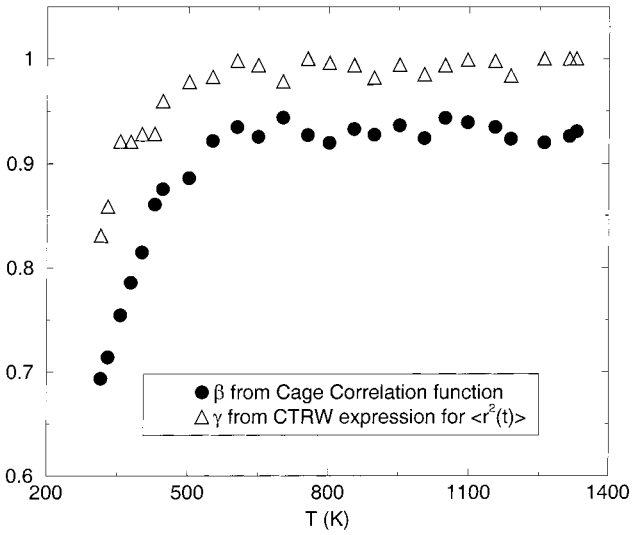

Figure 7. Comparison of exponential stretching coefficients, β from the cage-correlation function and γ from CTRW theory.

at all temperatures. In Figures 7 and 9, we show the effects of relaxing the linear fits of $\langle r^2(t)\rangle$ and of the long time portion of $ln[C_{cage}(t)]$. To fit the mean square displacements, we performed weighted nonlinear least-squaresd fits using the CTRW ($\gamma < 1$) expression for the mean square displacement (eq 7). The only free parameter in the fit is the jump distance, which we fixed at a value of 1.016 Å, the optimal jump distance for the $\gamma = 1$ case. These fits allow us to obtain estimates of γ and the hopping times τ directly from the mean square displacements. A sample of the a fit of the CTRW form of the $\langle r^2(t)\rangle$ (eq 7) at a temperature of 325K is shown in Figure 8.

The cage correlation functions were fit to the KWW law (eq 1), after correcting for the short-time (i.e., < 1 ps) vibrational decay. The values of γ from the $\langle r^2(t)\rangle$ fits are shown with the KWW stretching parameters in Figure 7. Note that fits for γ and the KWW stretching parameters both begin to show deviation from their more normal high-temperature behavior at approximately the same temperature as the appearance of the structural features (T_g^{WA}, and the split second peak in $g(r)$) noted above.

There is a small discrepancy between the stretching parameters (β) for the KWW fits and the values of γ for the CTRW fits to the time dependence of the mean-square displacement.

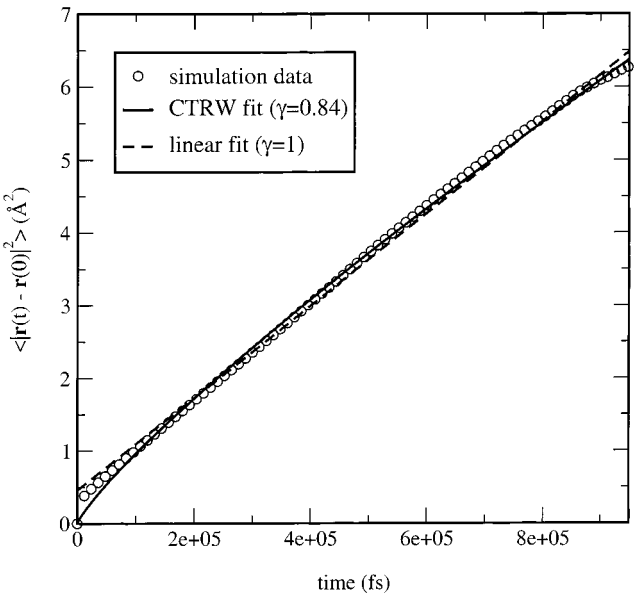

Figure 8. A fit of the mean square displacement at 325 K to the nonlinear form obtained via the CTRW model (eq 7).

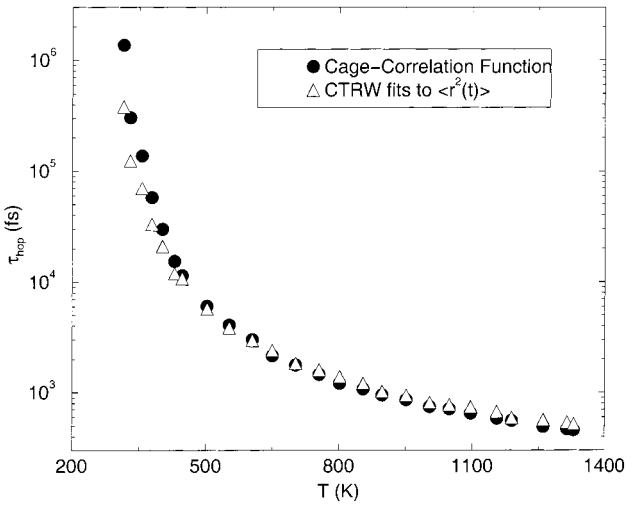

Figure 9. The characteristic hopping time, τ_{hop}, which characterizes the waiting time distribution. The solid circles represent hopping times predicted from KWW fits to the cage-correlation function. The open triangles represent the characteristic time calculated via the CTRW model for $\langle r^2(t)\rangle$.

Although there is not enough data to make a firm conclusion, it would appear that there is a small constant offset

$$\beta \approx \gamma - a \tag{18}$$

with $a \approx 0.06$ for this system. On the basis of the defect diffusion picture due to Blumen, Klafter, and Shlesinger,[27−29] one would expect that $\beta = \gamma$. The discrepancy could be due in part to the sensitivity of the cage correlation function to intermediate time scales (i.e., 10−30 ps). Observations at these times will be susceptible to the effects of short-lived inhomogeneities, whereas the CTRW fits (done over time scales from 10 ps − 1 ns) will show only the effects of inhomogeneities which persist for longer times. Because inhomogeneity can lead to the stretching behavior,[38] the values of the stretching parameter obtained from the longer time fits are the most relevant for understanding the process of vitrification.

In Figure 9, we show the hopping times for both models. As expected, the hopping times diverge as the temperature is

TABLE 1: Parameters for Sutton−Chen Many-Body Potential[a]

	D (meV)	c	m	n	α (Å)
Ag	4.0072	94.948	6	11	4.0691
Cu	5.7367	84.843	5	10	6.6030

lowered closer to the glass transition. There is relatively good agreement between the hopping times calculated via CTRW approach with those calculated via the cage correlation function, although the error is as much as a factor of 3 discrepancy at the lowest temperatures.

5. Discussion

It is relatively clear, from using the cage correlation function to obtain hopping times, that the CTRW approach to dispersive transport gives substantially better agreement than Zwanzig's model, which is based on interrupted harmonic motion in the inherent structures. The missing piece of the CTRW theory is the average hopping distance σ_0. A method for calculating σ_0 from short trajectories would make it much more useful for the calculation of diffusion constants in the $\gamma = 1$ limit.

In the low-temperature supercooled liquid, there are substantial deviations from the $\gamma = 1$ limit of the theory at temperatures below 500 K. Below this temperature, the mean square displacement cannot be fit well with a linear function in time, and the cage correlation function no longer has a simple exponential decay. In this paper, we have attempted to use the waiting time distribution due to Klafter et al.[15−18] The Laplace transform of eq 4 lends itself to the derivation of an analytical form for the propagator for dispersive transport.[16] However, it is somewhat troubling that the cage correlation function (which has proven itself to be a good indicator of the average decay of atoms from their initial sites) cannot be fit with a sticking probability that is commensurate with eq 4 without reverting to an intermediary defect diffusion model.[27−29]

Instead, we have been able to fit the long-time decay of the cage correlation function with the more familiar Kohlrausch−Williams−Watts law (eq 1), which appears to be a more accurate model for the sticking probability in this system. As formulated, the cage correlation function is a *direct* measure of the sticking probability for individual atoms, so there remains a troubling discrepancy in reconciling the CTRW approach to the data from our simulations. However, the similarity of the values for γ and β from these two different methods is evidence that there is a single mechanism underlying both the intermediate-time nonexponential decay of the cage correlation function and the long-time nondiffusive transport.

Acknowledgment. The authors would like to thank Donald Truhlar, Eran Rabani, and Bruce Berne for helpful discussions. This work has been supported in part by a New Faculty Award from the Camille and Henry Dreyfus Foundation.

References and Notes

(1) Pense, A. W. *Mater. Char*. **1992**, *29*, 213.
(2) Duwez, P.; Willens, R. H.; Klement, W. J. Jr. *Appl. Phys*. **1960**, *31*, 1136−1137.
(3) Peker, A.; Johnson, W. L. *Appl. Phys. Lett.* **1993**, *63*, 2342−2344.
(4) Kob, W.; Andersen, H. C. *Phys. Rev. E* **1995**, *51*, 4626−4641.
(5) Kob, W.; Andersen, H. C. *Phys. Rev. E* **1995**, *52*, 4134−4153.
(6) Sastry, S.; Debenedetti, P. G.; Stillinger, F. H. *Nature* **1998**, *393*, 554−557.
(7) Hansen, J. P.; McDonald, I. R. *Theory of Simple Liquids*; Academic Press: London, 1986.
(8) Gaukel, C.; Schober, H. R. *Solid State Comm*. **1998**, *107*, 1−5.
(9) Qi, Y.; Çağin, T.; Kimura, Y.; Goddard, W. A., III. *Phys. Rev. B* **1999**, *59*, 3527−3533.
(10) Rabani, E.; Gezelter, J. D.; Berne, B. J. *J. Chem. Phys.* **1997**, *107*, 6867−6876.
(11) Gezelter, J. D.; Rabani, E.; Berne, B. J. *J. Chem. Phys*. **1999**, *110*, 3444.
(12) Rabani, E.; Gezelter, J. D.; Berne, B. J. *Phys. Rev. Lett*. **1999**, *82*, 3649.
(13) Rabani, E.; Gezelter, J. D.; Berne, B. J. *Phys. Rev. Lett*. **2000**, *85*, 467.
(14) Zwanzig, R. J. *Chem. Phys*. **1983**, *79*, 4507−4508.
(15) Blumen, A.; Klafter, J.; Zumofen, G. *Phys. Rev. B* **1983**, *27*, 3429−3435.
(16) Klafter, J.; Zumofen, G. *J. Phys. Chem.* **1994**, *98*, 7366−7370.
(17) Klafter, J.; Shlesinger, M.; Zumofen, G. *Phys. Today* **1996**, *49*, 33−39.
(18) Shlesinger, M. F.; Klafter, J.; Zumofen, G. *Am. J. Phys.* **1999**, *67*, 1253−1259.
(19) Stillinger, F. H.; Weber, T. A. *Phys. Rev. A* **1982**, *25*, 978−989.
(20) Stillinger, F. H.; Weber, T. A. *Phys. Rev. A* **1983**, *28*, 2408−2416.
(21) Weber, T. A.; Stillinger, F. H. *J. Chem. Phys.* **1984**, *80*, 2742−2746.
(22) Stillinger, F. H.; Weber, T. A. *J. Chem. Phys.* **1985**, *83*, 4767−4775.
(23) Berne, B. J.; Pecora, R. *Dynamic Light Scattering*; Robert E. Krieger Publishing Company, Inc.: Malabar, Florida, 1990.
(24) Parkhurst, H. J., Jr.; Jonas, J. *J. Chem. Phys.* **1975**, *63*, 2698−2704.
(25) Parkhurst, H. J., Jr.; Jonas, J. *J. Chem. Phys*. **1975**, *63*, 2705−2709.
(26) Ngai, K. L.; Liu, F.-S. *Phys. Rev. B* **1981**, *24*, 1049−1065.
(27) Shlesinger, M. F.; Montroll, E. W. *Proc. Natl. Acad. Sci. U.S.A.* **1984**, *81*, 1280−1283.
(28) Blumen, A.; Klafter, J.; Zumofen, G. In *Fractals in Physics*; Peitronero, L., Tosatti, E., Eds.; International Symposium on Fractals in Physics, North-Holland: Amsterdam, 1986; Chapter 5, page 399.
(29) Klafter, J.; Shlesinger, M. F. *Proc. Natl. Acad. Sci. U.S.A.* **1986**, *83*, 848−851.
(30) Gezelter, J. D.; Rabani, E.; Berne, B. J. *J. Chem. Phys.* **1997**, *107*, 4618.
(31) Gezelter, J. D.; Rabani, E.; Berne, B. J. *J. Chem. Phys*. **1998**, *109*, 4695.
(32) Daw, M. S.; Baskes, M. I. *Phys. Rev. B* **1984**, *29*, 6443−6453.
(33) Sutton, A. P.; Chen, J. *Philos. Mag. Lett.* **1990**, *61*, 139−146.
(34) Lu, J.; Szpunar, J. A. *Philos. Mag. A* **1997**, *75*, 1057−1066.
(35) Alemany, M. M. G.; Rey, C.; Gallego, L. J. *J. Chem. Phys*. **1998**, *109*, 5175−5176.
(36) Belonoshko, A. B.; Ahuja, R.; Eriksson, O.; Johansson, B. *Phys. Rev. B* **2000**, *61*, 3838−3844.
(37) Banhart, J.; Ebert, H.; Kuentzler, R.; Voitländer, J. *Phys. Rev. B* **1992**, *46*, 9968−9975.
(38) Ediger, M.; Angell, C.; Nagel, S. R. *J. Phys. Chem.* **1996**, *100*, 13 200.
(39) Wendt, H.; Abraham, F. F. *Phys. Rev. Lett*. **1978**, *41*, 1244.
(40) Lewis, L. J. *Phys. Rev. B* **1991**, *44*, 4245−4254.
(41) Liu, R. S.; Qi, D. W.; Wang, S. *Phys. Rev. B* **1992**, *45*, 451−453.
(42) Truhlar, D. G.; Kohen, A., private correspondence.
(43) Tolman, R. C. *J. Am. Chem. Soc.* **1920**, *42*, 2506.
(44) Tolman, R. C. *Statistical Mechanics with Applications to Physics and Chemistry*; Chemical Catalog Co.: New York, 1927.